Magnetic exchange-coupling effects in asymmetric trilayer structures of MBE-grown Co/Cr/Fe

Katharina Theis-Bröhl, Rainer Scheidt, Thomas Zeidler, Frank Schreiber, and Hartmut Zabel
Ruhr-University Bochum, Institut für Experimentalphysik/Festkörperphysik, D-44780 Bochum, Germany

Thomas Mathieu, Christoph Mathieu,* and Burkard Hillebrands*
Universität Karlsruhe, Physikalisches Institut, Engesser Strasse 7, D-76128 Karlsruhe, Germany
(Received 1 June 1995; revised manuscript received 11 December 1995)

We present results of anisotropy and exchange-coupling studies of asymmetric Co/Cr/Fe trilayers and superlattices grown by molecular beam epitaxy on Cr(001)/Mg(001) buffers and substrates. The magnetic properties have been investigated using both the longitudinal magneto-optical Kerr effect and ferromagnetic resonance. The hysteresis data obtained from the trilayer system were fit to a theoretical model which contains both bilinear and biquadratic coupling. The effective in-plane anisotropy was found to be of fourfold symmetry with the same easy-axis orientation for both the Fe and Co layers. An analysis of the easy-axis hysteresis loops indicates long-period oscillatory coupling and also suggests a short periodic coupling. We show that weakly antiferromagnetically coupled asymmetric films might serve as potential candidates for improved spin-valve systems.

I. INTRODUCTION

Oscillatory exchange coupling has been discovered for different magnetic materials and a wide variety of nonmagnetic (NM) spacer materials over the last several years (for references see Ref. 1). The periods of the oscillations can be understood in terms of the electronic structure of the nonmagnetic spacer layer material.[2] However, some spacer materials like Cr or Mn are not completely ''nonmagnetic.'' In the case of Cr an antiferromagnetic (AF) structure of the moments is formed below the Néel temperature together with a spontaneous incommensurate collinear spin density wave. Therefore the exchange interaction between the Cr atomic planes should affect the coupling behavior of the adjacent magnetic layers as well. For the case of Fe/Cr(001), tight binding calculations[3] suggest AF interactions and, in the case of bcc Co/Cr(001), predict stable states for either ferromagnetic (FM) or AF alignment. Other calculations by Stoeffler *et al.*[4] predict parallel interactions in the case of the bcc Co/Cr(001) interface. But the interfacial magnetic coupling is predicted to be not very strong. That means that an antiparallel coupling is allowed in the case of a Co/Cr(001) interface whereas for Fe/Cr the parallel coupling does not exist.

Experimental investigations on high quality Fe/Cr(001) trilayers with short two monolayer (ML) period oscillations find the strongest AF maxima for even Cr spacer atomic layer (AL) numbers. These are 8 ML reported by Purcell *et al.*[5] and ≈ 4 ML reported by Demokritov *et al.*[6] However, if the magnetic layers are different on either side of the Cr spacer, then the AF maxima are expected at odd AL numbers.

Noncoupled multilayers consisting of two different magnetic materials with different coercitivities (which are separated by thick nonmagnetic spacers) have been studied for the purpose of using them as spin-valve systems.[7,8] These multilayers are magnetically uncoupled. However, an AF alignment of the moments can be obtained because of the different coercitivities of the two magnetic materials. Therefore, in the magnetic field range between the two flip fields a giant magnetoresistance can be found for some material combinations.[7–10]

II. SAMPLE PREPARATION

To study the coupling behavior of a system similar to Fe/Cr(001) but with a different second FM/NM interface a Co/Cr/Fe trilayer was grown with a wedge-shaped Cr interlayer. To grow the films a conventional 3-in. RIBER EVA 32 metal molecular beam epitaxy (MBE) system (equipped with two electron beam hearths and three ports for effusion cells) was used. One of the electron beam evaporators contains four rotable crucibles so that a total of eight different

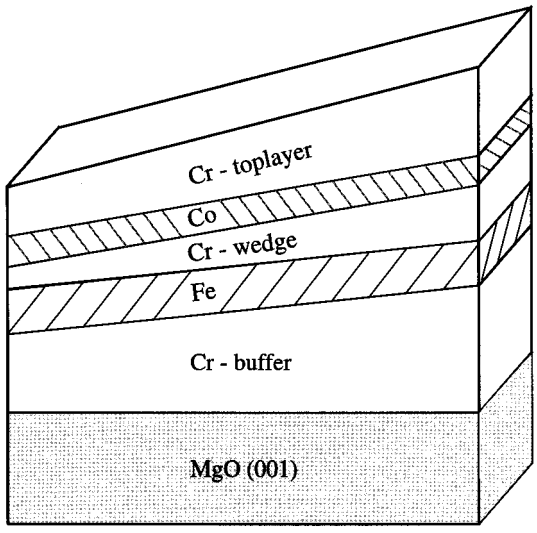

FIG. 1. Sequence of the (Co/Cr-wedge/Fe) film grown on Cr/MgO (001).

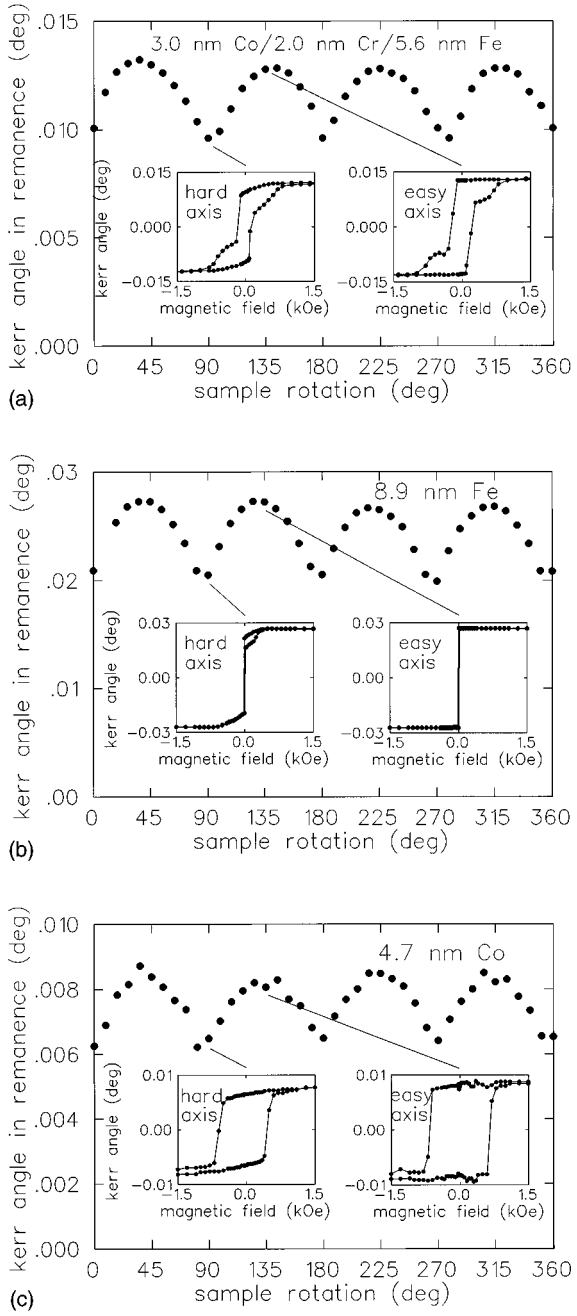

FIG. 2. Scans of the Kerr angle in remanence as a function of the sample rotation. Data from the MOKE hysteresis loops were taken during a complete sample rotation. The insets show the hard-axis (at minimum remanence) and easy-axis (at maximum remanence) hysteresis loops of the (Co/Cr-wedge/Fe) trilayer for 2.0 nm Cr layer thickness (a), a single 8.9-nm-thick Fe layer (b), and a 4.7-nm-thick Co-layer (c). Both single layers are embedded in Cr.

materials can be evaporated from this system. The vacuum base pressure of the system is below 5×10^{-9} Pa and the working pressure is better than 2×10^{-8} Pa .

The effusion cells contain 39-cm^3 crucibles providing a flux of a high stability. Therefore the film thickness could be established accurately by the evaporation time at a known growth rate. The flux of the materials which are evaporated from electron beam hearths is measured optically and controlled electronically during evaporation, and the shutters are

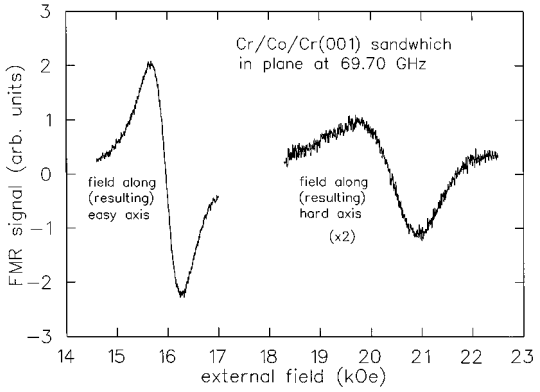

FIG. 3. FMR spectra of a 6.6-nm-thick single Co($11\overline{2}0$) layer. The resonance line with the external field along the hard axis corresponds to the *c* axis of one domain and perpendicular to the *c* axis of the other domain (right); the resonance line with the external field along the easy axis is measured at 45° with respect to the *c* axes.

computer controlled. We evaporated Co from a 40-cm^3 electron beam hearth and Fe from one of the 14-cm^3 crucibles in the four-crucible gun. We used constant evaporation rates of 0.6 nm/min for Co and Fe and different rates between 0.26 nm/min and 1.6 nm/min for the Cr spacer layer depending on the sample location. Cr was evaporated from an effusion cell with a pyrolytic graphite crucible. For the control of the Cr evaporation, only the effusion cell main shutter (which is in some distance from the cells) was used in order to ensure a stable temperature in the effusion cell during growth. The placement of the effusion cells is inclined at a certain angle to the 3-in. sample holder so that sample rotating is necessary to ensure a homogeneously thick film. Without rotation a linear gradient of the film thickness would be obtained over the sample holder. We used this linear gradient for designing our wedge-shaped Cr spacer.

To grow this system epitaxially we employed MgO(001) substrates. Since these substrates often have a surface that is insufficiently smooth for epitaxial growth, we subsequently repeated the commercial mechanical polishing of these substrates. With the help of *ex situ* small-angle x-ray scattering measurements and *in situ* reflection high-energy electron diffraction (RHEED) we were able to verify the surface quality of our MgO substrates before starting the growth. After introducing a freshly polished MgO sample into the vacuum chamber we outgassed and finally annealed it for more than 1 h at 1000 °C.

Figure 1 shows the sequence of the sample we used for analyzing the anisotropy and coupling behavior. The first layer grown on the MgO substrate is a bcc Cr(001) buffer. The optimized substrate temperature is 500 °C. Subsequently we annealed the buffer layer for 30 min at 750 °C. The following layers are grown at a substrate temperature of 300 °C. These consist of a 5.6-nm-thick bcc Fe(001) layer followed by the wedge-shaped Cr(001) spacer layer. The thickness of the spacer ranges from 0.5 nm and 3.0 nm over a sample length of 50 mm. Fe and Cr are both bcc materials with similar lattice constants. Their lattices nearly perfectly match with a misfit of less than 1%.

For the Co layer we have chosen a film thickness of only

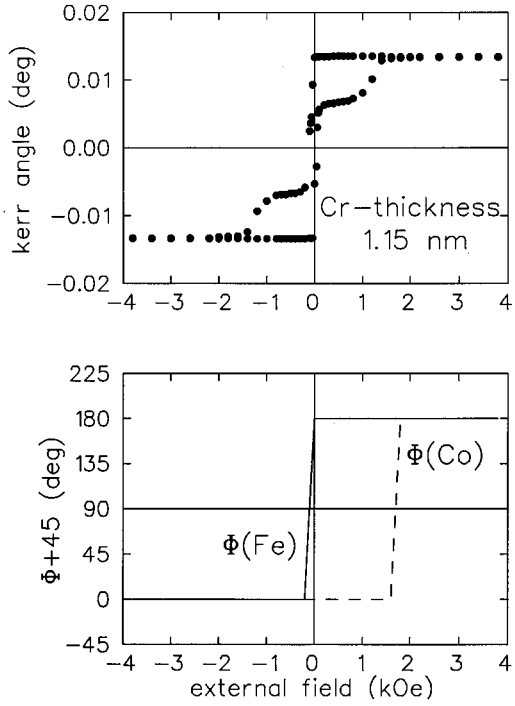

FIG. 4. The MOKE hysteresis loop for a Cr thickness of 1.15 nm measured at 45° (easy-axis configuration), showing a weak AF behavior (above), and the field dependence of the angles Φ_{Fe} and Φ_{Co} obtained from the fit (not shown) plotted for increasing field strength (below).

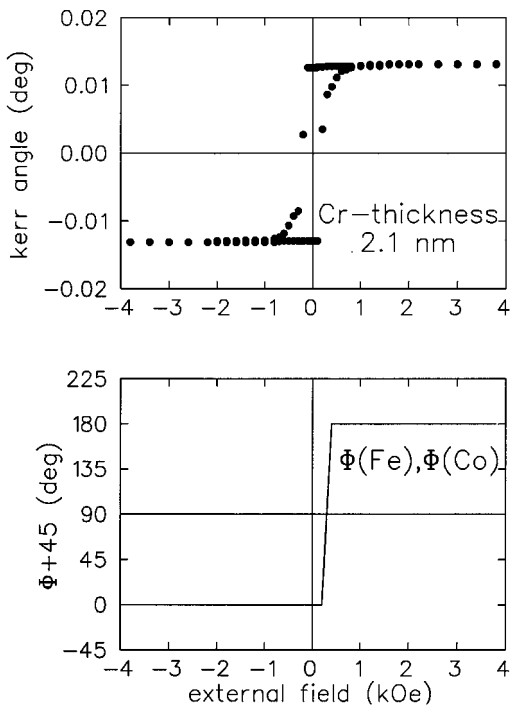

FIG. 5. The MOKE hysteresis loop for a Cr thickness of 2.10 nm measured at 45° (easy-axis configuration), showing a weak FM behavior (above), and the field dependence of the angles Φ_{Fe} and Φ_{Co} obtained from the fit (not shown) plotted for increasing field strength (below).

3.0 nm because of the strong in-plane anisotropy. The Co layer grows in the hcp phase in the $(11\bar{2}0)$ orientation with the c axis lying in the film plane. Since the uniaxial $(11\bar{2}0)$ Co structure is grown on bcc Cr(001) with a fourfold crystallographic symmetry, there are two equivalent orientations for the Co to grow with the c axis parallel to the $[110]$ and $[1\bar{1}0]$ axes of the Cr, respectively. This results in a twined crystallographic domain structure.[11] On the Co film we have grown a Cr top layer to prevent oxidation of the Co film. Oxidation investigations of thin Cr layers have shown that Cr oxidizes not more than 1.0 nm deep at room temperature.[12]

To check the total film thicknesses we used the thickness fringes of small-angle x-ray scans at different sample positions. Although we have grown a wedge-shaped sample, we calculated the total film thicknesses from the peak positions of the maxima of the thickness fringes (we used only maxima at $2\theta > 2°$ to minimize the size of the radiated area over the wedge). For these peak positions ($2\theta > 2°$) each calculated total film thickness deviates only slightly from the average thickness value. Unfortunately it was not possible to fit the small-angle x-ray data because of the strong angular depedence of the size of the radiated sample area for small angles ($2\theta < 2°$). By using additionally chemical x-ray fluorescence analysis the individual film thicknesses can be calculated for the different sample positions. This was possible because we have grown all individual Cr layers, including the buffer and the top layer, via the wedge shape. In this way the Cr growth rate exhibits a linear gradient across the sample which is constant during the entire film growth for each specific point of the sample. Because of the large sample length (50 mm), the gradient over the already wedge-shaped buffer layer (ranging from 5 to 30 nm) is not too large (1 ML increase in thickness at each 300 μm lateral distance). With these Cr-growth rates we were able to estimate the Cr spacer thicknesses from the total Cr thicknesses taking into consideration the proportions of the Cr-growth times.

With chemical x-ray fluorescence analysis we also checked the proportions of the individual materials over the entire sample and found that the Cr spacer thickness shows the expected linear gradient.

The structural measurements did not include studies of the interface roughness or possible interdiffusion. However, fits to high-angle x-ray diffraction data of Co$(11\bar{2}0)$/Cr(001) superlattices grown in the same MBE under the same conditions as the Co/Cr/Fe films should give reliable values for the interface roughness which was determined to $\sigma \approx 5$ Å.[13] Studies of Fe/Cr superlattices (grown in a different chamber) give an even smaller value for the interface roughness of $\sigma \approx 3.5$ Å.[14]

We have also grown samples with individual Co or Fe layers, respectively, embedded in Cr layers and superlattices with ten periodicities of the sequence of (Cr/Co/Cr/Fe). In these cases we used the sample rotation option during growth to get homogeneous Cr thicknesses over the films.

III. MOKE MEASUREMENTS

To study the magnetic properties of the Co/Cr/Fe sandwich sample we measured hysteresis loops with the

magneto-optical Kerr effect (MOKE) in the longitudinal configuration as a function of the Cr interlayer thickness by moving the laser spot along the wedge-shaped sandwich. The MOKE setup is described elsewhere.[15] The laser spot of a linear polarized He-Ne laser was focused to a diameter of 100 μm. We have chosen an incidence angle of the laser light of about 45° to the sample surface. Therefore the measurements are sensitive to the in-plane component of the magnetization. The reflected laser beam passes through a modulator and a rotator using the magneto-optical Faraday effect to measure quantitatively the Kerr rotation angle. The relatively high modulation amplitude and the use of lock-in techniques provides an angular resolution of better than 10^{-4} deg.

For each Cr thickness we performed a complete in-plane sample rotation and we measured hysteresis loops at every 9° of sample rotation to determine the easy and hard axes. For measuring the hysteresis loops we used a maximum magnetic field of 5.0 kOe. By plotting the Kerr angle in remanence as a function of sample orientation, indicated by the angle Φ_H of the external field with respect to the Cr[001] in-plane direction, a fourfold anisotropy was obtained. In Fig. 2(a) we present such a plot for the (Co/Cr/Fe) trilayer with Cr spacer thickness of 2.0 nm. The hysteresis loops show a nearly uncoupled behavior [insets of Fig. 2(a)] for this case. We also show plots of an individual 8.9-nm-thick Fe layer [Fig. 2(b)] and an individual 4.7-nm-thick Co layer [Fig. 2(c)]. Note the much higher coercitivity of the Co layer.

The maxima of the Kerr angles in remanence mark the in-plane easy axes. For Fe films they correspond to the crystallographic [100] and [010] directions; this reflects the well-known result of a positive cubic anisotropy parameter K_1^{cub} (Ref. 16) in [001] oriented films. In the case of Co, a fourfold anisotropy was measured as well. The hard axes are found to be along the [110] and [$1\bar{1}0$] axes which are *parallel* to the Co *c* axes and thus parallel to the hard in-plane axes of the Fe film. This behavior was found recently for Co($11\bar{2}0$) on Cr(001)/Nb(001)/Al_2O_3($1\bar{1}02$) by ferromagnetic resonance (FMR) measurements (see below and in Ref. 17).

In order to analyze the coupling behavior we performed MOKE hysteresis measurements at different points over the wedge-shaped trilayer sample. We discuss their behavior below.

IV. FMR MEASUREMENTS

To investigate further the nature of the fourfold anisotropy of Co in these samples FMR measurements were carried out on (Cr/Co/Cr/Fe) superlattices as well as on individual Fe and Co layers embedded in (001)Cr layers using the same setup as described in Ref. 17. All samples were grown on a Cr(001) buffer layer on MgO(001) substrates.

All samples show an almost perfect fourfold in-plane anisotropy. This result can be readily understood if one assumes equal film areas for both in-plane growth orientations of Co. The uniaxial anisotropy contribution of hcp Co with the *c* axis as the easy axis is averaged out due to the 90° orientation of the *c* axes of the two growth orientations. The next higher anisotropy contribution in hcp symmetry, K_2^{hcp}, which is of fourfold symmetry, is observed as the lowest-order contribution.[17]

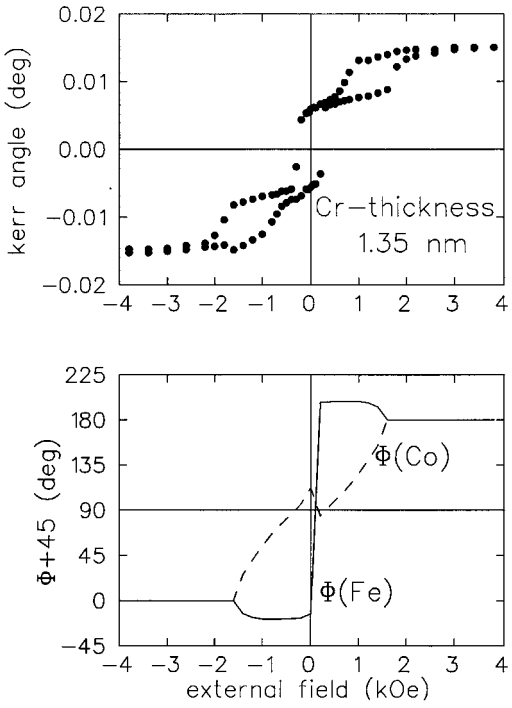

FIG. 6. The MOKE hysteresis loop for a Cr thickness of 1.35 nm measured at 45° (easy-axis configuration), showing a strong AF behavior (above), and the field dependence of the angles Φ_{Fe} and Φ_{Co} obtained from the fit (not shown) plotted for increasing field strength (below).

To discuss the Co behavior in more detail we show the resonance spectra of a single Co($11\bar{2}0$) layer with a thickness of 6.6 nm (see Fig. 3). A purely fourfold anisotropy can be concluded from the observation of about the same spectra after each 90° sample rotation. To estimate the areal difference of the portion of both growth orientations we use the difference of the line positions of FMR spectra at Φ_H and $(\Phi_H+90°)$ which is less than 0.1 kOe. From this value the difference is estimated to be less than $\approx$2% using the relations given in Ref. 17.

Only one resonance line at each easy-axis orientation was found in the FMR spectra of the Co layers. This indicates that the crystallographic Co growth domains are much smaller in size than the magnetic domains; i.e., the crystallographic domains can be treated in the limit of strong magnetic coupling.[17] In the opposite case, two lines would be observed. For the case found here, and with a nearly 1:1 proportion of the Co-growth domains, the resulting anisotropy energy is $F_{\mathrm{ani}}^{\mathrm{eff}}=\frac{1}{2}F_{\mathrm{ani}}^{\mathrm{eff}}(\Phi)+\frac{1}{2}F_{\mathrm{ani}}^{\mathrm{eff}}(\Phi+90°)$ with contributions from the two growth domains of $F_{\mathrm{ani}}^{\mathrm{eff}}(\Phi)$ and $F_{\mathrm{ani}}^{\mathrm{eff}}(\Phi+90°)$. Here Φ is the in-plane angle of the direction of magnetization measured against the in-plane Cr[001] axis. The resulting in-plane anisotropy is fourfold and has the same shape as that for cubic in-plane anisotropies. The hcp anisotropy constant K_2 is in this case the relevant parameter for the anisotropy expression. If $K_2>0$, the easy axis will then be found *between* the two *c* axes. Therefore, neglecting the out-of-plane Θ dependence, we can write the anisotropy energy (as for the Co case[17])

TABLE I. Results of the FMR measurements for individual Co and Fe layers and superlattices. For the purpose of comparison, also the Fe bulk values are given.

Sample	t_{Fe}	t_{Co}	$4\pi M_{eff}$	$4\pi M^*_{eff}$	$2K_1/M$	K_2^{eff}/M
Co sandwich		6.6 nm		14.5 kOe		1.5 kOe
Co sandwich		4.7 nm		14.5 kOe		1.8 kOe
$(Cr/Co/Cr/Fe)_{10}$	3.2 nm	2.6 nm	21.0 kOe		0.40 kOe	
$(Cr/Co/Cr/Fe)_{10}$	2.4 nm	2.0 nm	21.6 kOe		0.53 kOe	
Fe sandwich	3.0 nm		21.84 kOe		0.54 kOe	
Fe sandwich	8.9 nm		21.98 kOe		0.60 kOe	
Fe bulk			21.49 kOe		0.55 kOe	

$$F_{ani}^{eff}=\frac{1}{8}K_2\cos[4(\Phi+45°)]$$
$$=-K_2\sin^2(\Phi+45°)\cos^2(\Phi+45°)+\text{ const}$$
$$=K_2\sin^2(\Phi)\cos^2(\Phi)+\text{const.} \quad (1)$$

The angular offset of 45° accounts for the rotation of the c axes from the [100] axes. Table I shows the results of the anisotropy parameters including the effective magnetization which is defined as

$$4\pi M^*_{eff}=4\pi M_s-2\frac{2K_s}{2Mt_{Co}}+\frac{K_1^{hcp}}{M}+\frac{2K_2^{hcp}}{M} \quad (2)$$

for the $(11\bar{2}0)$-oriented Co layers (following the notation of Ref. 17). For the present thickness range, the K_s term is of minor importance. The results for the Fe(001) individual layers show almost bulklike behavior. $4\pi M_{eff}$ for Fe is defined in the usual manner collecting all $\sin^2\Theta$ contributions of the energy expression. The behavior of the (Cr/Co/Cr/Fe) superlattices is apparently dominated by the Fe layers. The result of the fits of the FMR data for both Co samples yields $4\pi M_{eff}=14.5$ kG. This value is in good agreement with the bulk value, taking into consideration the bulk value of $K_1/M\approx$ 3 kOe and $2K_2/M\approx$ 1–2 kOe and neglecting surface anisotropy effects for this thickness.

V. DISCUSSION

To analyze the MOKE hysteresis loops of the wedged-shaped Co/Cr/Fe sandwich (see Figs. 4–7) we tried to fit our data of the hard- and easy-axis loops. We assumed the following expression for the free energy, neglecting constant terms:

$$F_{mag}=[-\mu_0 M^{Fe}H\cos(\Phi_{Fe}-\Phi_H)+K_1^{Fe}\sin^2\Phi_{Fe}\cos^2\Phi_{Fe}]t_{Fe}$$
$$+[-\mu_0 M^{Co}H\cos(\Phi_{Co}-\Phi_H)$$
$$+K_2^{Co}\sin^2\Phi_{Co}\cos^2\Phi_{Co}]t_{Co}$$
$$-2A_{12}\cos(\Phi_{Fe}-\Phi_{Co})-2B_{12}\cos^2(\Phi_{Fe}-\Phi_{Co}). \quad (3)$$

To minimize the free energy a simplex algorithm was used. The algorithm guarantees that after every field step the next local minimum is searched.

For very small Cr layer thicknesses (t_{Cr} = 0.55–0.75 nm) a simultaneous fit to the data of the easy and hard axes was possible. Unfortunately, the fits to the data for thicker Cr spacers do not yield a uniform set of parameters for both axes. The theoretically expected steps in the hysteresis loops are too much rounded out in our experimental data. Responsible for this are probably domain processes which are not included in our model. For small Cr thicknesses the strong ferromagnetic coupling suppresses the formation of domains.

For Cr spacers thicker than 0.75 nm fits to the data of the MOKE hysteresis loops with the external field applied along the easy-axis direction at 135° provide information on the coupling constants as well as on the alignment of the Fe and Co moments. These fits to the easy-axis loops are in reasonable agreement mainly for those parts of the loops at which no domain nucleation processes and domain wall movements determine the magnetization behavior.

Taking into consideration the different thicknesses (5.6 nm for Fe and 3.0 nm for Co), the product of the saturation magnetization (assuming bulklike behavior) and the layer thickness ($M_s t$) in the external field term of the free energy is about twice as high for the Fe layer as for the Co layer. Therefore the behavior of the Fe layer is expected to be influenced much stronger by the external field than that of the Co layer. This is demonstrated by the results of the fits for Φ_{Fe} and Φ_{Co} of the easy-axis hysteresis loops (see Figs. 4–7).

In particular, the Fe moments flip already at small (reverse) magnetic fields while the moments in the Co layer remain in the original direction. Apparently, the magnetization of the Co layer follows the rotation of the Fe layer and not the external field. In addition the much higher coercitivity of individual Co layers (see Fig. 2) leads to the conclusion that Co must undergo a much more complicated domain structure. Due to the different magnetic behavior of Fe and Co [see Figs. 2(b) and (c)], a nearly uncoupled Co/Cr/Fe trilayer shows hysteresis loops which are close to those shown in Figs. 2(a) for t_{Cr}=2.0 nm.

The fits for the Cr thickness of t_{Cr}=2.0 nm reveal the absence of bilinear coupling (A_{12}=0) and a weak biquadratic coupling ($B_{12}=-0.01$ mJ/m^2). Because the high coercitivity of the Co layer is not included in our model, this biquadratic coupling value of $B_{12}=-0.01$ mJ/m^2 might represent the Co coercitivity and not a ''real'' biquadratic coupling.

The shapes of the easy-axis hysteresis loops for a weak AF coupling differ from those with a nearly uncoupled behavior mainly by a longer step in the loop for the former case. In Fig. 4 we present an easy-axis hysteresis loop for weakly AF coupled Co and Fe layers at a Cr thickness

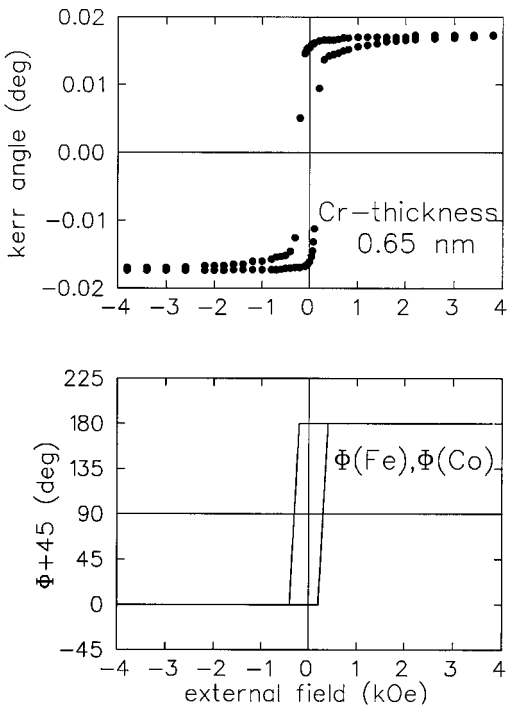

FIG. 7. The MOKE hysteresis loop for a Cr thickness of 0.65 nm measured at 45° (easy-axis configuration), showing a FM behavior (above), and the field dependence of the angles Φ_{Fe} and Φ_{Co} obtained from the fit (not shown) plotted for increasing field strength (below).

t_{Cr}=1.15 nm (with the fit results $A_{12}=-0.03$ mJ/m^2, $B_{12}=-0.01$ mJ/m^2). In comparison, for a weak FM coupling strength the length of the step decreases or the step nearly vanishes (see Fig. 5). It is interesting to note that the length of the step is very sensitive to the coupling behavior. Slight variations of the coupling constants in the case of a weak coupling behavior (FM or AF) produce drastic changes of the step length [compare Figs. 4 and 5 and insets of Figs. 2(a) and 8]. Also the flip field of the Fe moments undergoes changes with the coupling characteristics. A systematic change can be obtained in the case of a weak coupling beavior when the flip of the Fe moments occurs before the Co moments change their alignment. For a weak AF coupling the flip of the Fe moments may occur at slightly negative magnetic fields, at zero field, or very small positive fields. For zero coupling or a weak FM coupling the flip of the Fe moments occurs at slightly higher positive magnetic fields.

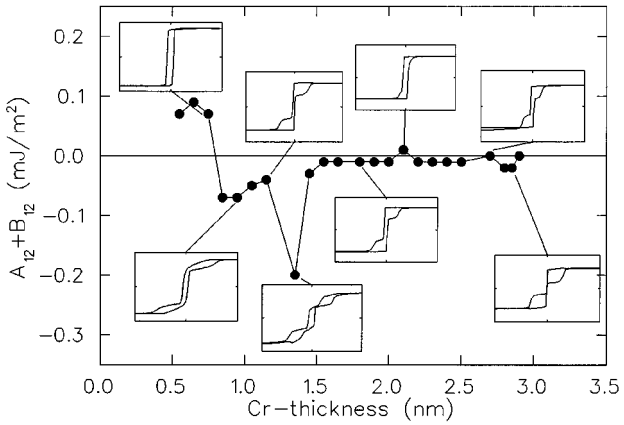

FIG. 8. Results of our fits to the data for $A_{12}+B_{12}$ as a function of the Cr spacer thickness. The insets show the shapes of the hysteresis loops measured at different Cr thicknesses.

The behavior of these weak AF coupled asymmetric trilayers is very interesting for use as spin valves. By choosing the proper Cr spacer thickness the flip of the Fe moments can be tuned to occur at zero or at very small magnetic fields. The clear step in the hysteresis loops after the flip of the Fe moments occurs indicates the AF alignment of the moments of the Fe and Co layers over a wide magnetic field range (δ H $\approx$ 1 kOe for the hysteresis loop shown in Fig. 4). The weak AF coupling should also be interesting for other spin-valve systems since it could solve the problem of finding a material with an extremely small coercitivity for spin-valve systems. By tuning the first spin flip to about zero field by using the proper spacer thickness the expected flip behavior for ideal spin valves could be reached.

In all cases of our (Co/Cr/Fe) trilayer with weak coupling characteristics, the Co moments first remain in their original alignment after the flip of the Fe moments occurs. With increasing field domain and/or rotation processes of the moments occur. For a larger AF coupling the Co moments change their alignment before the flip of the Fe moments occurs (see Fig. 6). For a Cr thickness of 1.35 nm the strongest AF coupling constants were found ($A_{12}=-0.12$ mJ/m^2 and $B_{12}=-0.08$ mJ/m^2). Note that a high biquadratic coupling constant B_{12} (compared to A_{12}) is obtained. For Cr thicknesses between 0.85 nm and 1.05 nm, the shapes of the hysteresis loops again suggest a strong AF coupling. For this region we found coupling constants of ($A_{12}+B_{12}=-0.05$ to -0.07 mJ/m^2). In this case the biquadratic coupling constant B_{12} is much higher than the bilinear one A_{12} (see Table II).

For a strong FM coupling we find hysteresis loops without any steps and a clear FM shape. In this case the Co layer couples so strongly to the Fe with FM moment alignment that the magnetization processes of both materials occur together. Such loops can be obtained at t_{Cr}=0.55 nm and t_{Cr}=0.75 nm. At t_{Cr}=0.65 nm the shape of the hysteresis loops suggests that the Co moments do not reach complete saturation after the flip (see Fig. 7). For all three Cr layer thicknesses the fits give a positive coupling constant A_{12}=0.07–0.09 mJ/m^2.

In Fig. 8 we present the results of our simulations for the coupling constants $A_{12}+B_{12}$ as a function of the Cr spacer thickness. A long-period coupling oscillation with a period of 10–11 ML is deduced from the two AF maxima at $\approx$9 ML and $\approx$20 ML and from the FM maxima at 4–5 ML and $\approx$15 ML. The second-long period AF maxima at t_{Cr}=2.85 nm ($A_{12}=-0.01$ mJ/m^2 and $B_{12}=-0.01$ mJ/m^2) also can be deduced clearly from the shapes of the hysteresis loops in this Cr region (see insets of Fig. 8). Also a 2-ML short-period coupling might exist in this system. We obtained two strong AF maxima at $\approx$7 ML and $\approx$9 ML, separated by a region with weak coupling characteristics. But in other Cr thickness regions no short-period coupling can be found.

The odd Cr atomic layer number suggests a ferromagnetic Co/Cr interface exchange coupling (parallel alignment of moments), assuming an antiferromagnetic exchange for the Fe/Cr interface.

TABLE II. Results of the fits to the MOKE hysteresis loops for Cr thicknesses.

t_{Cr} (nm)	t_{Cr} (ML)	A_{12} (mJ/m^2)	B_{12} (mJ/m^2)	$A_{12}+B_{12}$ (mJ/m^2)
0.55 nm	3.8 ML	+0.07	0	+0.07
0.65 nm	4.5 ML	+0.09	0	+0.09
0.75 nm	5.2 ML	+0.07	0	+0.07
0.85 nm	5.9 ML	0	-0.07	-0.07
0.95 nm	6.6 ML	-0.02	-0.05	-0.07
1.05 nm	7.3 ML	0	-0.05	-0.05
1.15 nm	8.0 ML	-0.03	-0.01	-0.04
1.35 nm	9.4 ML	-0.12	-0.08	-0.20
1.45 nm	10.0 ML	0	-0.03	-0.03
1.55–2.00 nm	10.8–13.9 ML	0	-0.01	-0.01
2.10 nm	14.6 ML	+0.02	-0.01	+0.01
2.20–2.50 nm	15.3–17.4 ML	0	-0.01	-0.01
2.70 nm	18.8 ML	0	0	0
2.80–2.85 nm	19.4–19.8 ML	-0.01	-0.01	-0.02
2.90 nm	20.1 ML	0	0	0

In the case of Fe/Cr, biquadratic coupling can be observed mostly in a region between the AF and the FM maxima (see Ref. 18). But our fits to the data for the Co/Cr/Fe trilayer system suggest that the highest negative biquadratic coupling constant B_{12} occurs at the strong AF maxima. As previously mentioned the coupling constant $B_{12}=-0.01$ mJ/m^2 found (from the simulations) for most of the hysteresis loops in the case of a weak coupling may represent the coercitivity of the Co layer. The strong biquadratic coupling constants found at the AF maxima should be reduced by this value. This does not influence the main behavior.

VI. CONCLUSION

In conclusion, we have studied the magnetic properties of (Co/Cr/Fe) samples, as well as individual Co and Fe layers, by the MOKE and FMR. We suggest coupled crystallographic (1120)Co domains with an almost 1:1 distribution of both domains causing a fourfold anisotropy behavior of the Co layer, with similar characteristics as for the Fe layer. The MOKE hysteresis loops show an indication of a long-period (10–11 ML) and a short-period (2 ML) exchange coupling oscillation, with the AF maxima at odd numbers of AL's of the Cr spacer. The strongest AF maximum (with a coupling constant of -0.20 mJ/m^2) was found at 9 ML. The fits to the data also reveal a high biquadratic constant whenever the AF coupling shows maxima.

In the case of a zero or a weak coupling behavior both magnetic materials (Fe and Co) show different flip fields. After the first flip (Fe) an AF alignment between the Fe and the Co moments can be obtained. The flip of the Fe moments (the material with the smaller coercitivity) can be tuned to about zero field by choosing the proper Cr spacer layer thickness in the case of a weak AF coupling. Those asymmetric films with weak AF coupling behavior can be used as ideal spin-valve systems.

ACKNOWLEDGMENTS

The authors wish to thank W. Oswald, J. Podschwadek, and P. Stauche for technical help. We wish also to thank Z. Frait (Prague) for the use of his FMR spectrometer for additional measurements. The work was supported by the Deutsche Forschungsgemeinschaft through SFB 166. One of us (K.T.B.) thanks M. B. Salamon for helpful discussions and C. P. Flynn for hospitality and acknowledges partial support from the Physics Department at the University of Illinois at Urbana-Champaign.

*Present address: Fachbereich Physik, Universität Kaiserslautern, Erwin-Schrödinger-Straße 46, 67663 Kaiserslautern, Germany.

[1] M.D. Stiles, Phys. Rev. B **48**, 7738 (1993).

[2] K.B. Hathaway, in *Ultrathin Magnetic Structures II*, edited by B. Heinrich and J.A.C. Bland (Springer-Verlag, Berlin, 1994).

[3] J.H. Hasegawa, Phys. Rev. B **42**, 2368 (1990); **43**, 10 803 (1990).

[4] D. Stoeffler and G. Gautier, J. Magn. Magn. Mater. **104-107**, 1819 (1992); Phys. Rev. B **44**, 10 389 (1991); Surf. Sci. **251/252**, 31 (1991).

[5] S.T. Purcell, W. Folkerts, M.T. Johnson, N.W.E. McGee, K. Jager, J. Aan de Steege, W.P. Zeper, and P. Grünberg, Phys. Rev. Lett. **67**, 903 (1991).

[6] S. Demokritov, J.A. Wolf, P. Grünberg, and W. Zinn, in *Magnetic Thin Films, Multilayers and Surfaces*, edited by S.S.P. Parkin, MRS Symposia Proceedings No. 231 (Materials Research Society, Pittsburgh, 1991).

[7] T. Shinjo and H. Yamamoto, J. Phys. Soc. Jpn. **59**, 3061 (1990); H. Yamamoto, T. Okuyama, H. Dohnomae, and T. Shinjo, J. Magn. Magn. Mater. **99**, 243 (1991).

[8] B. Dieny, V.S. Speriosu, S.S.P. Parkin, B.A. Gurnay, D.R. Wilhoit, and D. Mauri, Phys. Rev. B **43**, 1297 (1991).

[9] P.P. Freitas, J.L. Leal, T.S. Plaskett, and L.V. Melo, J. Appl. Phys. **75**, 6480 (1994).

[10] H. Hosoya, M. Komoto, and Y. Sugita, J. Magn. Soc. Jpn. **18**, 341 (1994).

[11] N. Metoki, W. Donner, and H. Zabel, Phys. Rev. B **49**, 17 351

(1994); W. Donner, N. Metoki, A. Abromeit, and H. Zabel, Phys. Rev. B **48**, 14 745 (1993).
[12] A. Stierle (private communication).
[13] W. Donner, Ph.D. thesis, Ruhr-Universiät Bochum, Germany, 1994.
[14] A. Schreyer, J.F. Ankner, Th. Zeidler, H. Zabel, R. Schäfer, J.A. Wolf, P. Grünberg, and C.F. Majkrzak, Phys. Rev. B **52**, 16 066 (1995).
[15] N. Metoki, Th. Zeidler, A. Stierle, K. Bröhl, and H. Zabel, J. Magn. Magn. Mater. **118**, 57 (1993).
[16] Th. Mhüge, Th. Zeidler, Q. Wang, Ch. Morawe, N. Metoki, and H. Zabel, J. Appl. Phys. **77**, 1055 (1995).
[17] F. Schreiber, Z. Frait, Th. Zeidler, N. Metoki, W. Donner, H. Zabel, and J. Pelzl, Phys. Rev. B **51**, 2920 (1995).
[18] M. Rührig, R. Schäfer, A. Hubert, R. Mosler, J.A. Wolf, S. Demokritov, and P. Grünberg, Phys. Status Solidi A **125**, 635 (1991).